Supporting Information

Ag size/structure-dependent effect on low-temperature selective catalytic oxidation of NH_3 over Ag/MnO_2

Haifeng Wang[1], Mingyue Lin[2,3], Toru Murayama[2,3,4*], Shixiang Feng[1], Masatake Haruta[2], Hiroki Miura[1,3,5], Tetsuya Shishido[1,2,3,5*]

[1]Department of Applied Chemistry for Environment, Graduate School of Urban Environmental Sciences, Tokyo Metropolitan University, 1-1 Minami-Osawa, Hachioji, Tokyo 192-0397, Japan

[2]Research Center for Gold Chemistry, Tokyo Metropolitan University, Tokyo, 192-0397, Japan

[3]Research Center for Hydrogen Energy-based Society, Tokyo Metropolitan University, Tokyo 192-0397, Japan

[4]Yantai Key Laboratory of Gold Catalysis and Engineering, Shandong Applied Research Center of Gold Nanotechnology (Au-SDARC), School of Chemistry & Chemical Engineering, Yantai University, Yantai 264005, China

[5]Elements Strategy Initiative for Catalysts & Batteries, Kyoto University, Kyoto, 615-8520, Japan

Corresponding Authors

Email for Tetsuya Shishido: shishido-tetsuya@tmu.ac.jp

Email for Toru Murayama: murayama@tmu.ac.jp

This PDF file includes:

1. Supplementary Methods

1.1 Catalyst preparation

Ag/MnO_2 catalysts were prepared by a multi-step process. Firstly, rod-shaped MnO_2 was synthesized by a hydrothermal method. In detail, 2.484 g $MnSO_4 \cdot H_2O$ and 1.659 g $KMnO_4$ were dissolved in 75 mL deionized water and then put into a 100 mL Teflon-lined stainless steel autoclave that was sealed and maintained at 160 ºC for 24 h. The resulting black slurry was filtered, washed with 2 L deionized water, and then dried at 120 ºC for 24 h, followed by calcination at 500 ºC in a furnace for 6 h at a ramp of 5 ºC/min for further use. Secondly, 2.0 g MnO_2 was weighed and added to 100 mL H_2O and stirred in an ice bath for 1 h. Then 0.315 g $AgNO_3$ was initially dissolved in 20 mL deionized water to form a transparent solution, to which 0.3 mL 25 wt% ammonia solution was added dropwise with stirring, resulting in another transparent $[Ag(NH_3)_2]OH$ solution. Subsequently, both the $[Ag(NH_3)_2]OH$ solution and an H_2O_2 solution (30 wt.%, 30 mL) were added simultaneously and drop by drop to an MnO_2 suspension and stirred at 0ºC for 3 h. After that, the final suspension was filtered, washed with 500 mL distilled water, and then dried at 80 ºC for 24 h to obtain the Ag/MnO_2-80 precursor. Then Ag/MnO_2-80 was calcined at 200, 300, 400 and 500 ºC for 6 h at a ramp of 5 ºC/min in a furnace to obtain Ag/MnO_2-200, Ag/MnO_2-300, Ag/MnO_2-400 and Ag/MnO_2-500 samples, respectively. Note that the Ag loading was set as 10 wt% unless otherwise stated. These catalysts were referred to as Ag/MnO_2-X (where *X* indicates calcination temperatures of 200, 300, 400 and 500ºC, respectively).

Other catalysts with 5 wt%, 20 wt% and 30 wt% Ag loadings and calcination at 400 ºC were also synthesized for investigation of the effect of Ag loadings. They were referred to as yAg/MnO_2-400 (where y indicates the Ag loading)

1.2 **Catalyst characterizations**

1.2.1 Atomic absorption spectra

Atomic absorption spectra (AAS) was obtained by using a Shimadzu AA-6200 to estimate the actual loading amount of Ag on the surface of Ag/MnO_2-*X* catalysts. Prior

to the measurement, ~20 mg sample was dissolved in newly prepared 0.5 mol/L HNO_3 solution for 10 min with shaking, and then the solution was adjusted with distilled water to 20 mL for measurement. Standard Ag solutions of 1.094 mg/L, 2.1875 mg/L, 4.375 mg/L, 8.75 mg/L and 17.5 mg/L were used for the creation of a calibration curve.

1.2.2 Transmission electron microscopy

The morphology, mean size and height of Ag nanoparticles were investigated by high-resolution transmission electron microscopy (JEOL, JEM-3200FS) at 300 kV. Samples were deposited on a carbon film-coated mesh copper grid. At least 150 particles were measured in different areas to determine the mean particle diameter and size distribution of each sample.

1.2.3 Powder X-ray diffraction

Powder X-ray diffraction (XRD) patterns of the samples were collected on a Rigaku Smartlab with Cu- Kα radiation (λ = 1.5418 Å). XRD data were taken over the 2 theta range from 10º to 80º at a scan rate of 2º min^{-1}.

1.2.4 XAFS

Ag K-edge XAFS measurements were performed at the BL01B1 beamline at SPring-8 (Hyogo, Japan) operated at 8 GeV using a Si (311) two-crystal monochromator. XAFS spectra were obtained at room temperature. XAFS data were processed to isolate EXAFS spectra from the background using Athena software. Replicate scans were averaged to increase the signal-to-noise ratios. The resulting EXAFS spectra (*k* space) were Fourier-transformed and fitted in R space using Artemis software.

1.2.5 NH_3-TPD

The acid properties of supports were measured by temperature-programmed desorption of ammonia (NH_3-TPD) using a Belcat system equipped with a mass spectrometer detector (BEL Japan). Prior to the measurement, the sample (ca. 50 mg) was preheated under helium (50 mL/min) at 200 °C for 1 h (at 80 ºC for the Ag/MnO_2-80 catalyst). Then 5% NH_3/He was introduced at 25 °C for 30 min. Finally, the NH_3 desorption profile from 25 °C to 700 °C was recorded with a mass spectrometer under 30 mL/min He flow.

1.2.6 O_2-TPD

Temperature-programmed desorption of oxygen (O_2-TPD) was carried out using a Belcat system equipped with a mass spectrometer detector (BEL Japan). Prior to the measurement, the sample (ca. 30 mg) was preheated under helium (50 mL/min) at 200 °C for 1 h (at 80 ºC for the Ag/MnO_2-80 catalyst). Then 30 mL/min 5% O_2/He was introduced at 100 °C for 30 min. Finally, the O_2 desorption profile from 100 °C to 800 °C (700 ºC for the MnO_2 support) was recorded with a mass spectrometer under 30 mL/min He flow.

1.2.7 H_2-TPR

Temperature-programmed reduction of hydrogen (H_2-TPR) was carried out using a Belcat system equipped with a mass spectrometer detector (BEL Japan). Prior to the measurement, the sample (ca. 40 mg) was pretreated under 5% O_2 (50 mL/min) at 200 °C for 1 h (at 80 ºC for the Ag/MnO_2-80 catalyst). Then the H_2 reduction profile was recorded with a mass spectrometer in 50 mL/min 5% H_2/Ar flow from 40 °C to 600 °C

1.2.8 N_2 adsorption and desorption

The specific surface area and pore size distribution of Ag-based catalysts were determined from N_2 adsorption isotherms at -196 ºC on BELSORP. The analyzed samples were outgassed at 300 ºC for 3 h prior to the measurement.

1.3 NH_3-SCO reaction test

The catalysts were tested for NH_3-SCO reaction in a fixed-bed flow reactor (7.9 mm in diameter) using the Belcat II system under atmospheric pressure. The sample weight was set as 150 mg unless otherwise state. The composition of the gas mixture at the reactor inlet was NH_3 (100 ppm, 50 mL/min), O_2 (20 mL/min), and balance Ar (30 mL/min). The total flow rate of the reaction mixture was 100 mL/min with a space velocity (SV) of 40000 mL $h^{-1}g^{-1}$. The outlet gas compositions were analyzed with an online FTIR spectrometer (JASCO, FT-IR4700) equipped with a DTGS detector. The parameters used for calculations of conversion and selectivity were selected at the

steady state to exclude the influence of physically adsorbed NH_3 on the support.

NH_3 conversion and the selectivities to N_2, N_2O and NO were calculated using the following equations S1-S4:

$$NH_3\ \text{conversion}\ (\%) = \frac{NH_{3(in)} - NH_{3(out)}}{NH_{3(in)}} \times 100\% \quad (S1)$$

$$N_2\ \text{selectivity}\ (\%) = \frac{NH_{3(in)} - NH_{3(out)} - NO_{(out)} - NO_{2(out)} - 2N_2O_{(out)}}{NH_{3(in)} - NH_{3(out)}} \times 100\% \quad (S2)$$

$$N_2O\ \text{selectivity}\ (\%) = \frac{2N_2O_{(out)}}{NH_{3(in)} - NH_{3(out)}} \times 100\% \quad (S3)$$

$$NO\ \text{selectivity}\ (\%) = \frac{NO_{(out)}}{NH_{3(in)} - NH_{3(out)}} \times 100\% \quad (S4)$$

1.4 Kinetic measurements

Apparent activation energy

The calculation of apparent activation energy was based on linear-fitting data in Arrhenius plots with catalytic activity below 20% NH_3 conversion.

Reaction order

A catalyst of 150 mg was used for the study of reaction order. When O_2 reaction order was measured, the reaction temperature was set at 60 ºC. The concentration of NH_3 was kept constant at 50 ppm balanced with Ar. The O_2 concentration was varied from 5% to 20% (5%, 10%, 15% and 20%). When NH_3 reaction order was measured, the reaction temperature was set at 70 ºC. The concentration of O_2 was kept constant at 20% while the NH_3 concentration was varied from 50 ppm to 100 ppm (50, 60, 70, 80, 90 and 100 ppm).

1.5 Verification of the absence of internal diffusion limitations.

Weisz – Prater Criterion (C_{WP}): [1]

$$C_{WP} = \frac{\text{Reaction rate}}{\text{Diffusion rate}} = \frac{-r'_{A(meas)}\rho_c R^2}{D_e C_{As}} < 0.3 \quad (S5)$$

Where $r'_{A(meas)}$ is the measured reaction rate (mol/g • s), ρ_c is the catalyst packing

density (g/cm^3), R is the catalyst particle radius (cm), D_e is the gas phase diffusivity (cm^2/s) and C_{As} is the ammonia concentration at the catalyst surface (mol/cm^3).

The values of Weisz – Prater Criterion (C_{WP}) over the Ag/MnO_2-400 catalyst at various temperatures were calculated, and the results are shown in Table S1. The calculated values are far less than 0.3, indicating that mass transfer limitations can be ignored in this work.

Table S1. Weisz – Prater Criterion (C_{WP}) values at various temperatures

Temp. (°C)	$r'_{A(meas)}$ (mol/g· s)	D_e (cm^2/s)	C_{As} (mol/cm^3)	Weisz-Prater criterion
35	2.2E-09	45794.96	1.98E-09	0.00005
40	2.7E-09	46914.61	1.95E-09	0.00006
45	2.8E-09	48043.24	1.92E-09	0.00007
50	3.9E-09	49180.78	1.89E-09	0.00009
55	5.2E-09	50327.16	1.86E-09	0.00013
60	7.1E-09	51482.31	1.83E-09	0.00017
70	8.7E-09	53818.65	1.78E-09	0.00021
75	1.3E-08	54999.72	1.75E-09	0.00033
80	1.8E-08	56189.31	1.73E-09	0.00044
85	2.2E-08	57387.35	1.70E-09	0.00054
90	2.3E-08	58593.79	1.68E-09	0.00058
100	2.3E-08	61031.62	1.63E-09	0.00058
110	2.3E-08	63502.35	1.59E-09	0.00059
120	2.3E-08	66005.55	1.55E-09	0.00060

The detailed calculation steps and parameters are shown below:

Table S2. Parameters used for Weisz – Prater criteria

Observed reaction rate $r'_{A(meas)}$	$NH_3\ conversion\ \times \frac{NH_3\ flow\ rate\ (\frac{mol}{s})}{Amount\ of\ catalyst(g)}$ $= NH_3\ conversion \times$ [2.28 $\times 10^{-2}$ mol g^{-1} s^{-1}]
NH_3 concentration at the catalyst surface (as a function of temperature) C_{As}	$\frac{N_{NH_3}}{V}$ [mol cm^{-3}] $= \frac{1}{T}$ [2.45$\times 10^{-3}$ K·mol cm^{-3}]
Catalyst packing density ρ_c	0.1 [g cm^{-3}]
Catalyst particle radius R	0.002 [cm]

The diffusivity (D_e) can be calculated as follows

$$D_e = \frac{1}{1/D_b + 1/D_{Kn}} \qquad \text{(S6)}$$

where D_b is the bulk diffusivity and D_{Kn} is the Knudsen diffusivity.

The bulk diffusivity (D_b) is given by:

$$D_b = \frac{\bar{v}\lambda_g}{3} \qquad \text{(S7)}$$

Where λ_g is the mean free path in the gas phase, $\bar{v}$ is the mean velocity.

The Knudsen diffusivity (D_{Kn}) is given by:

$$D_{Kn} = \bar{v}\frac{d_p}{3} \qquad \text{(S8)}$$

Where d_p is the pore diameter of the catalyst (4.3 nm).

The mean free path in the gas phase is calculated by:

$$\lambda_g = \frac{1}{\sqrt{2}\pi\sigma^2(N_{NH_3}/V)} = \frac{RT}{\sqrt{2}\pi\sigma^2 P_{NH_3}} \qquad \text{(S9)}$$

where σ is the molecular diameter of NH_3 (2.90×10^{-8} cm), [2] R is the universal gas constant ($82.057 * \frac{atm \cdot cm3}{K \cdot mol}$), P_{NH_3} is the NH_3 partial pressure (5.07×10^{-6} mol%.). Thus,

the mean free path as a function of temperature becomes:

$$\lambda_g = \frac{RT}{\sqrt{2}\pi\sigma^2 P_{NH_3}} = (7.288 \times 10^{-4}) * T \frac{cm}{K} \quad \text{(S10)}$$

For example, the mean free path at a reaction temperature of 50 °C is 0.236 cm (or 2.355 $\times 10^{6}$ nm), which is far greater than the pore diameter (4.3 nm) of the catalysts. Hence, pore diffusion is dominated by Knudsen diffusion.

$$D_e \cong D_{Kn} \quad \text{(S11)}$$

The mean velocity for the NH_3 molecule is given by:

$$\bar{v} = \left(\frac{8k_B T}{\pi m}\right)^{1/2} \quad \text{(S12)}$$

Where k_B is the Boltzmann's constant (1.381×10^{-16} g cm^2 s^{-2} K^{-1}) and m is the mass of NH_3 (17 amu = 2.824×10^{-23} g). Hence, the mean velocity for the NH_3 molecule as a function of temperature

$$\bar{v} = 1.2459 \times 10^7 \, T^{1/2} \frac{cm}{s \cdot K^{1/2}} \quad \text{(S13)}$$

Therefore, the effective diffusivity becomes:

$$D_e = 1.7443 \times 10^7 \, T^{1/2} \frac{cm^2}{s \cdot K^{1/2}} \quad \text{(S14)}$$

2. Supplementary Discussion

2.1. Supplementary information on Ag/MnO_2 catalysts

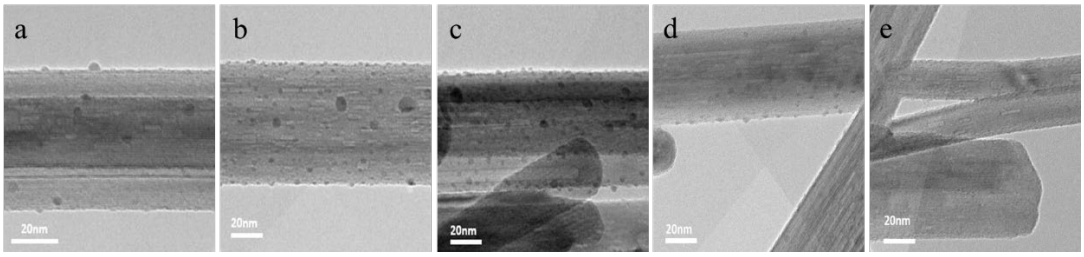

Fig. S1. TEM images of Ag/MnO_2-*X* catalysts: (a) Ag/MnO_2-80, (b) Ag/MnO_2-200, (c) Ag/MnO_2-300, (d) Ag/MnO_2-400, and (e) Ag/MnO_2-500.

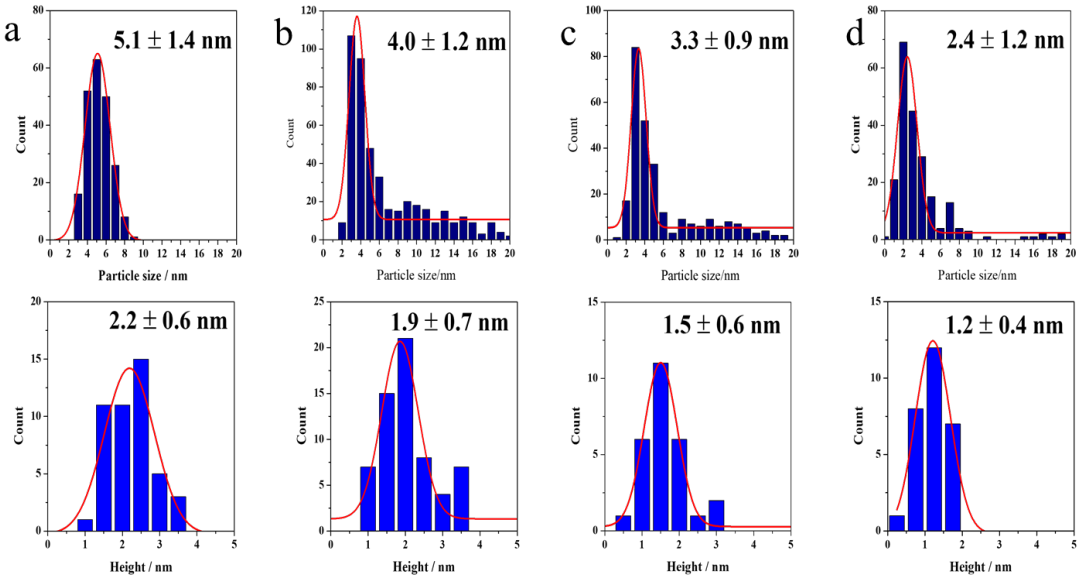

Fig. S2. Particle size distributions (upper) and height distributions (lower) of Ag/MnO_2-*X* catalysts: (a) Ag/MnO_2-80, (b) Ag/MnO_2-200, (c) Ag/MnO_2-300, and (d) Ag/MnO_2-400.

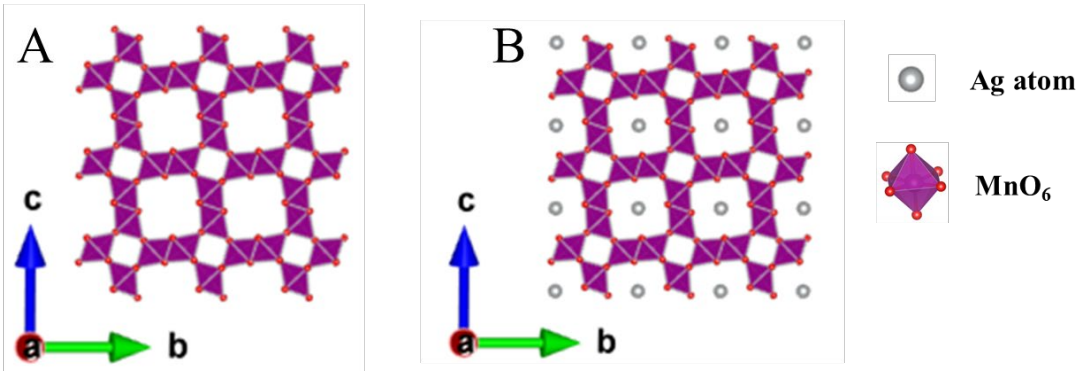

Fig. S3. The cross-sectional views of model structures of MnO_2 and Ag/MnO_2-500 catalysts.

Rod-shaped MnO_2 with a width of about 80 nm can be clearly seen in Fig. S1 regardless of the calcination temperature from 80 ºC to 500 ºC, suggesting that the calcination process after Ag deposition did not change the morphology of the MnO_2 support, and the rod morphology of the MnO_2 support remained for all of the catalysts tested.

The Ag NPs with a narrow size distribution were deposited on the rod-shaped MnO_2 in Ag/MnO_2-*X* catalysts (Fig. S2). The size of the Ag NPs on MnO_2 that was dried at 80 ºC was about 5.1 nm, and no obvious larger aggregates were found over Ag/MnO_2-80. In addition, the Ag NPs gradually became smaller with increase in the calcination temperature up to 400 ºC. Atomically dispersed Ag might be formed at a temperature of 500 ºC, at which no obvious Ag NPs were observed by HR-TEM, being consistent with previous reports. The average heights of Ag nanoparticles over various catalysts were also measured (Fig. S2). The average height gradually decreased from 2.2 nm (for Ag/MnO_2-80) to 1.2 nm (for Ag/MnO_2-400) with increase in the calcination temperature up to 400 ºC. The height can't be measured over Ag/MnO_2-500 catalyst because atomically dispersed Ag atoms formed in/on the channel structure of MnO_2 support.

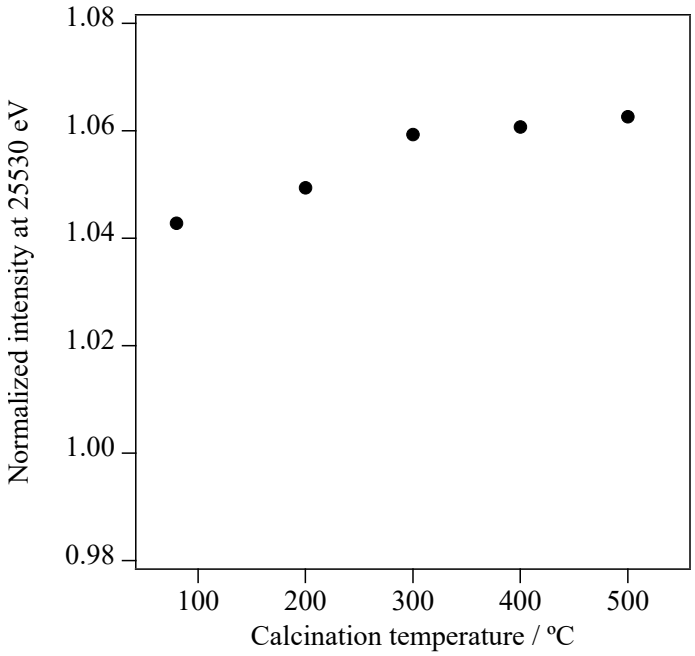

Fig. S4. White-line intensity of Ag K-edge XANES spectra of Ag/MnO_2-*X* catalysts at 25530 eV. For Ag foil, the intensity is 0.98566.

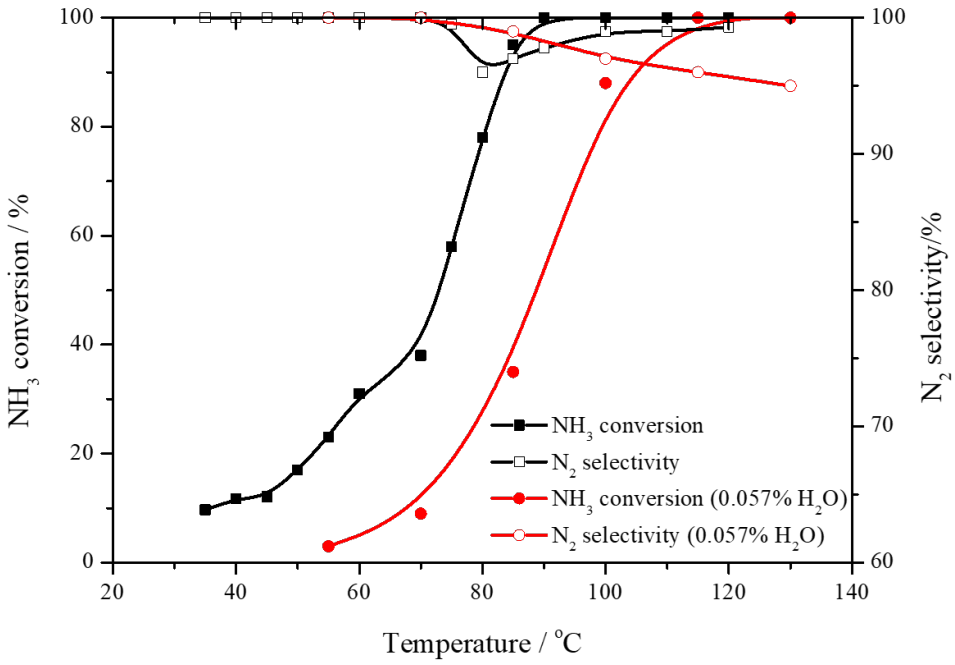

Fig. S5. The influence of H_2O on NH_3-SCO over the Ag/MnO_2-400 catalyst in the presence/absence of H_2O in reaction gas as a function of temperature. H_2O concentration: 0.057 %; 50 ppm NH_3; 20% O_2; 100 mL/min.

Fig. S5 shows the influence of H_2O on NH_3-SCO catalytic performance over Ag/MnO_2-400 catalyst. As it can be seen, NH_3 oxidation activity decreased with the presence of 0.057% H_2O in the inlet reaction gas. The temperature of 100% NH_3 conversion increased by around 25 °C after the introduction of H_2O. Besides, N_2 selectivity slightly decreased from 99% to 96% in the presence of H_2O at 115 °C. These results indicated that H_2O might adsorb on the catalyst surface and block the active sites for NH_3 oxidation but only has a little effect on N_2 selectivity over Ag/MnO_2-400 catalyst.

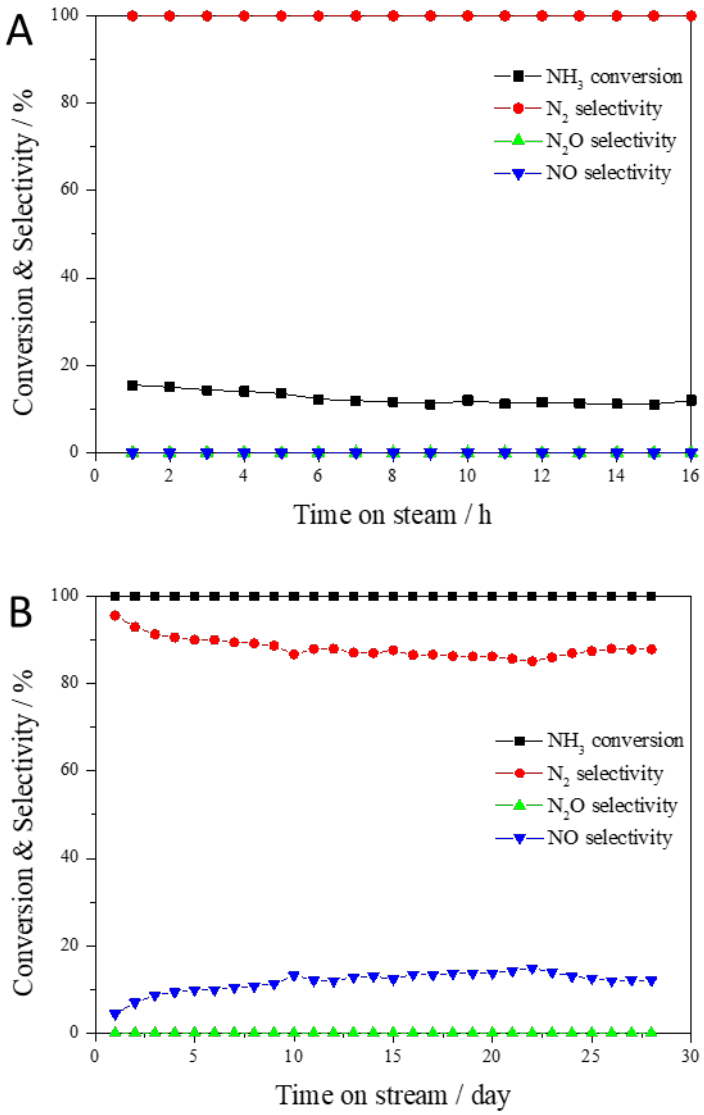

Fig. S6. Stability test over the Ag/MnO_2-400 catalyst at 40 ºC (A) and 125 ºC (B)

Stability tests over Ag/MnO_2-400 at 40 ºC and 125 ºC were carried out. As shown in Fig. S6, it was found that NH_3 conversion initially was 15% at 40 ºC and remained at 12%-15% for 16 hours without obvious decrease in NH_3 conversion. Moreover, no N_2O and NO were formed during the stability test, N_2 selectivity remained at 100% all the time. Besides, as shown in Fig. S6B, it was found that NH_3 conversion reached 100% at 125 ºC and remained at that conversion for near one month. Meanwhile, N_2 selectivity kept at around 90% for about 20 days.

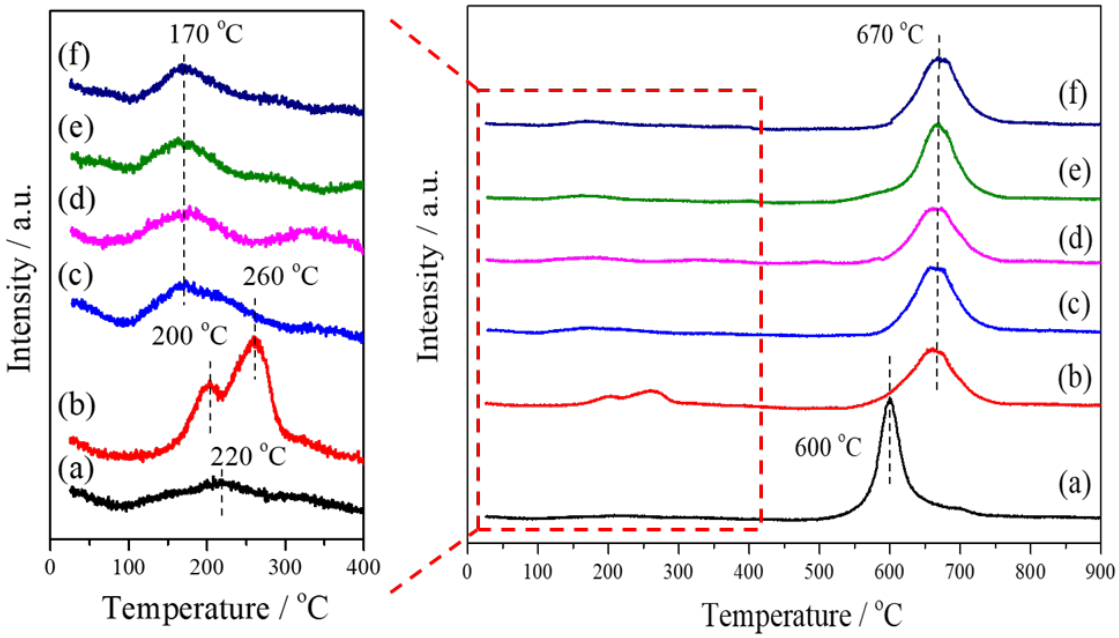

Fig. S7. NH_3-TPD profiles of Ag/MnO_2-*X* catalysts: (a) MnO_2, (b) Ag/MnO_2-80, (c) Ag/MnO_2-200, (d) Ag/MnO_2-300, (e) Ag/MnO_2-400 and (f) Ag/MnO_2-500.

The acidity properties of the strength and amount of acid sites of the catalysts and supports were studied by NH_3-TPD measurements, and the results are shown in Fig. S7. Obvious desorption peaks appeared at temperatures of 500-700 °C. The temperature of NH_3 desorption on MnO_2 appeared at 600 °C, and the desorption peak shifted to 670 °C after Ag deposition for Ag/MnO_2-*X* catalysts regardless of the calcination temperature, indicating that the Ag NPs were mainly located at strong Lewis acid sites, thereby forming stronger acid sites, possibly around the periphery over Ag/MnO_2-*X*. At temperatures lower than 400 °C, as shown in the magnification inset, one small NH_3 desorption peak over MnO_2 appeared at 220 °C, and the peak shifted to a lower position than MnO_2, indicating that a few weak acid sites were also formed over Ag/MnO_2-*X* catalysts, possibly due to weak NH_3 adsorption over Ag NPs. Recently, acid sites including Brønsted and Lewis sites have been found to participate in the ammonia oxidation reaction, thus improving catalytic activity. Weakly bonded NH_3 is more active than strongly bonded NH_3 in the NH_3 oxidation reaction, and these weak acid

sites that formed after deposition of Ag might therefore have contributed to the increase in the catalytic activity in a low temperature range. Nevertheless, the small increase in weak acid sites cannot fully explain the significant increase in NH_3 catalytic oxidation activity.

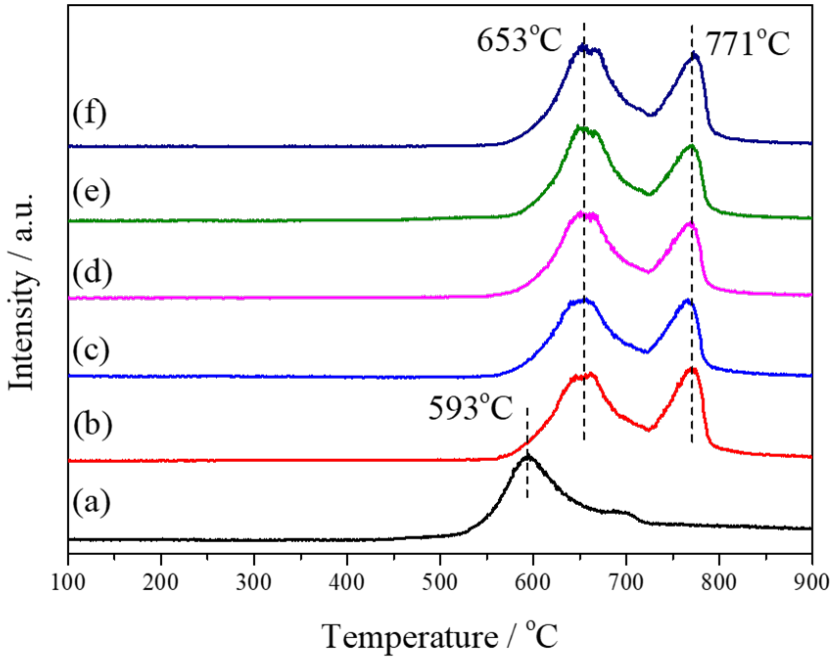

Fig. S8. O_2-TPD profiles of Ag/MnO_2-*X* catalysts: (a) MnO_2, (b) Ag/MnO_2-80, (c) Ag/MnO_2-200, (d) Ag/MnO_2-300, (e) Ag/MnO_2-400 and (f) Ag/MnO_2-500.

O_2-TPD measurements were carried out to investigate the O_2 capacity and desorption property. As shown in Fig. S8, the temperature of O_2 desorption of MnO_2 appeared at 593 °C, and the O_2 desorption peaks shifted to 653 °C and 771 °C after deposition of Ag, indicating that O_2 adsorption was enhanced by introduction of Ag. Besides, there is no apparent differences in the peak positions of Ag/MnO_2-*X* catalysts regardless of the calcination temperature, suggesting that O_2 adsorption and desorption over Ag/MnO_2-*X* were not the main reason for the increase in NH_3 catalytic oxidation activity.

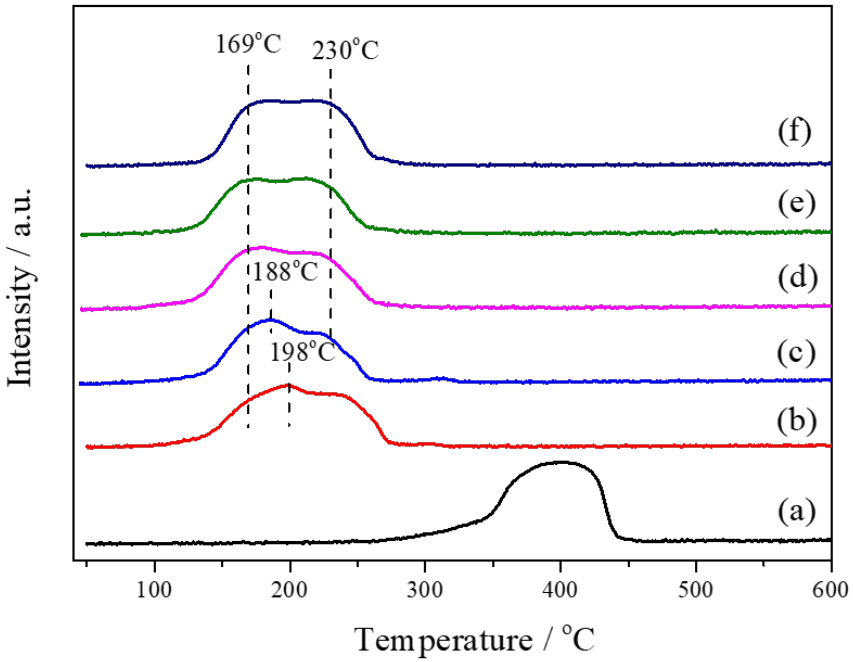

Fig. S9. H_2-TPR profiles of Ag/MnO_2-*X* catalysts: (a) MnO_2, (b) Ag/MnO_2-80, (c) Ag/MnO_2-200, (d) Ag/MnO_2-300, (e) Ag/MnO_2-400 and (f) Ag/MnO_2-500.

H_2-TPR were carried out to obtain information on the reducibility of the Ag-based catalysts, and the results are shown in Fig. S9. The lattice oxygen of MnO_2 is not active in an H_2 atmosphere at T < 250 °C, whereas Ag/MnO_2-*X* is active for H_2 oxidation at temperatures lower than 200 °C. An apparent increase in reducibility was found after introduction of Ag. It is known that the oxidation activity of Ag is positively associated with reducibility due to the enhanced O_2 activation property over a catalyst surface. Therefore, the increased reducibility can help to explain the improved catalytic activity. However, the large differences in NH_3 conversion and N_2 selectivity cannot be clearly explained by H_2-TPR measurement.

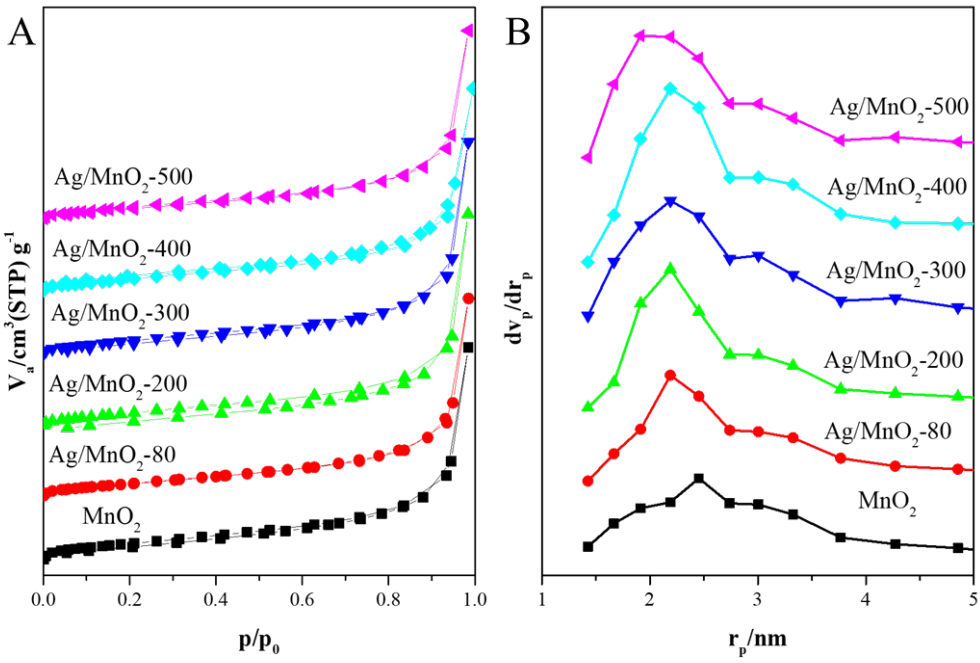

Fig. S10. N_2 adsorption and desorption isotherms (A) and pore size distributions (B) of Ag/MnO_2-*X* catalysts.

N_2 adsorption and desorption measurements were next conducted to examine the pore properties of the samples. Fig. S10 shows the N_2 adsorption and desorption isotherms and pore size distributions of Ag/MnO_2-*X* catalysts. The isotherms of all of the samples belonged to type II without an obvious hysteresis loop, indicating a nonporous structure. The Barrett−Joyner−Halenda (BJH) pore size distribution curve shows that the average pore size slightly decreased with increase in the calcination temperature, indirectly indicating that the Ag atoms migrated into channel structures of MnO_2, thus changing the channel structure.

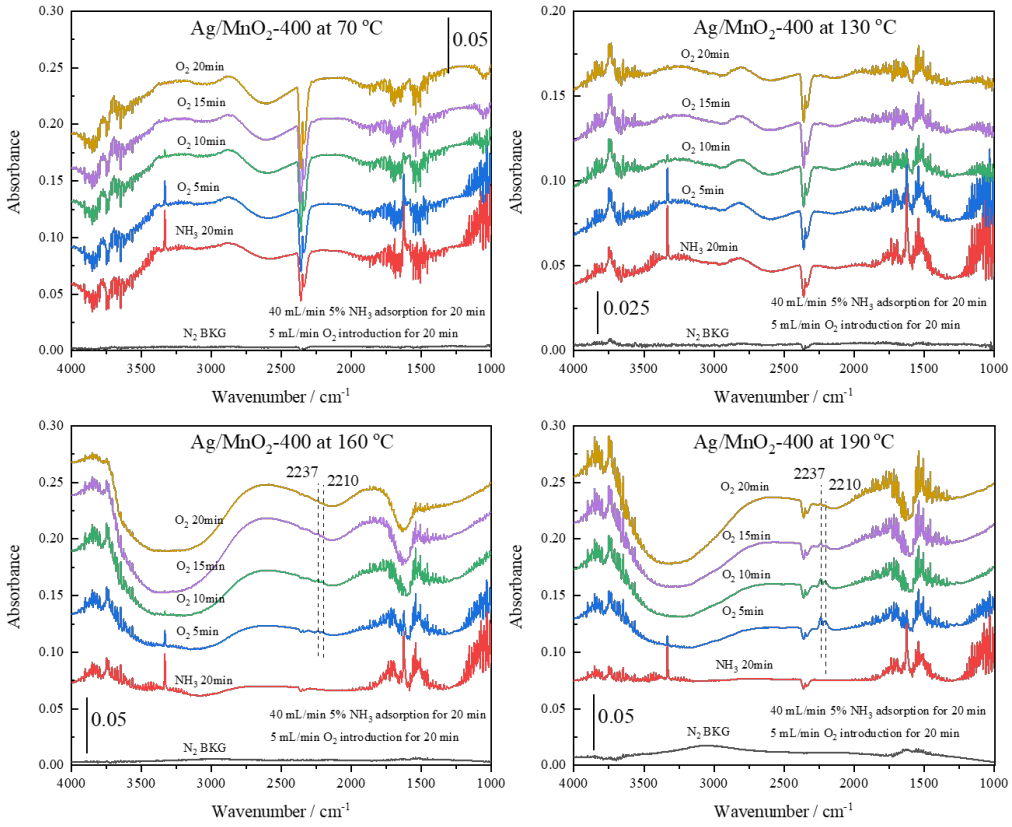

Fig. S11 *In-situ* NH_3 DRIFTS results of Ag/MnO_2-400 catalyst at various temperatures.

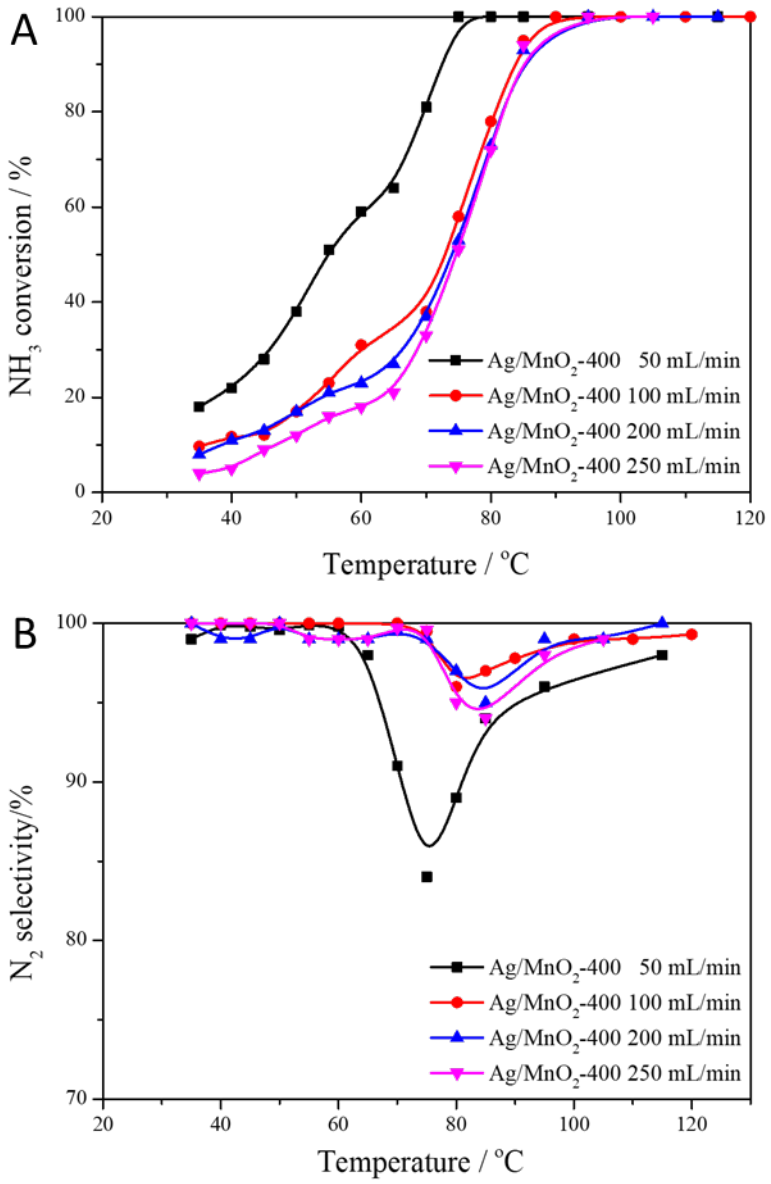

Fig. S12. Catalytic oxidation activity tests over Ag/MnO_2-400 catalysts with different flow rates.

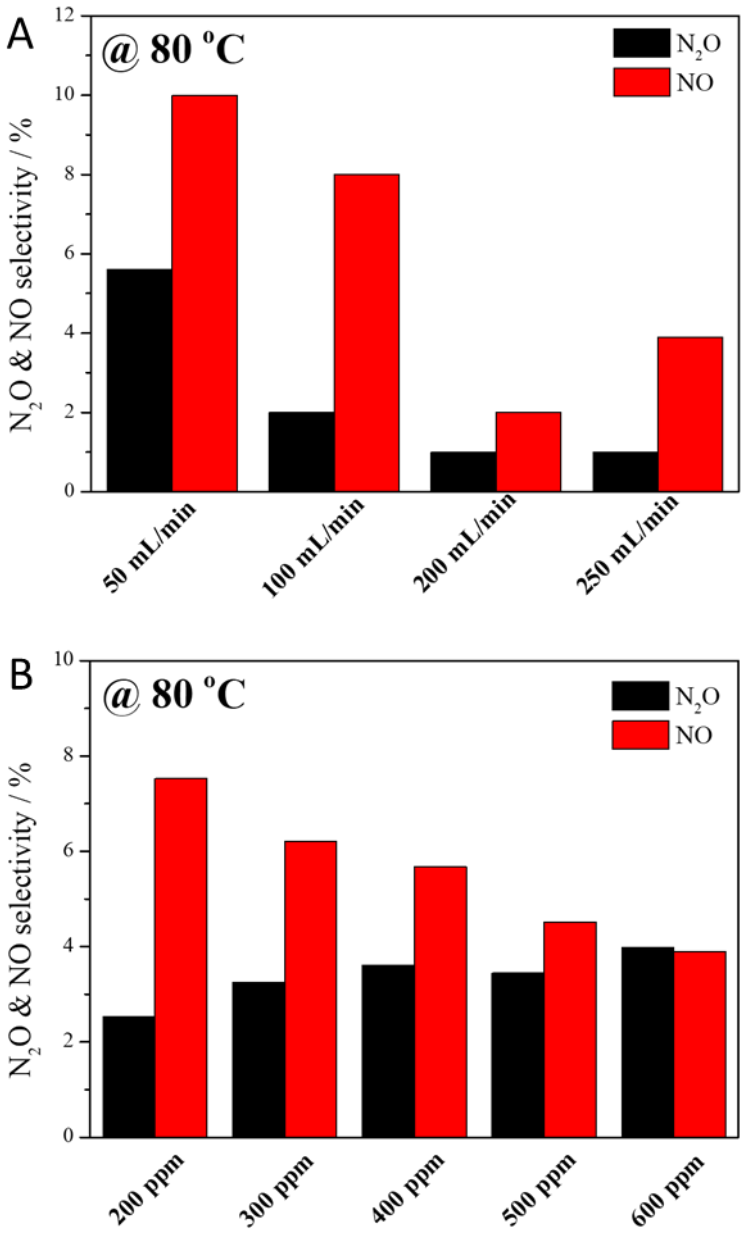

Fig. S13. N_2O and NO selectivities over Ag/MnO_2-400 catalysts at 80 ºC.

(A) NH_3 concentration of 50 ppm NH_3 (50 mL/min-200 mL/min).

(B) NH_3 concentration of 200-600 ppm NH_3 (100 mL/min).

The effect of flow rate on catalytic performance over Ag/MnO_2-400 was studied, and the results are shown in Fig. S12. Fig. S13 shows the N_2O and NO selectivities over Ag/MnO_2-400 catalysts at 80 ºC with different flow rates (A) and different inlet NH_3 concentrations (B). As shown in Fig. S12, the catalytic activity was decreased by

increasing the flow rate from 50 mL/min to 200 mL/min, indicating that the residence time of reactants has an influence on catalytic activity. Interestingly, the selectivity of N_2O and NO decreased from 15% to 5%, that is, the N_2 selectivity was increased from 84% to more than 95% with an increase in the flow rate from 50 mL/min to 200 mL/min (Fig. S13A). This phenomenon suggests that the flow rate has a positive effect on N_2 selectivity by decreasing the formation of NO and N_2O byproducts, possibly because one of the intermediates can react with NH_3 to form N_2. Fig. S13B shows the effect of inlet NH_3 concentration on N_2 selectivity over Ag/MnO_2-400 catalysts at 80 ºC with a total flow rate of 100 mL/min. The results showed that N_2 selectivity was slightly improved by increasing the inlet NH_3 concentration from 200 ppm to 600 ppm. A tendency for NO selectivity to decrease was also found when the inlet NH_3 concentration was increased from 200 ppm to 600 ppm.

Table S3. Overview of literature data of catalytic performance related to Ag based catalysts

Catalyst	Reaction condition	Conversion (%) /Temperature (°C)	N_2 selectivity/ (%)/ Temperature (°C)	Published year	Ref.
Ag powder	[NH_3]=1000 ppm, [O_2]=10%, Flow rate=50 mL/min, weight=0.1 g	100%/200 °C	38%/200 °C	2001	3
10 wt% Ag/Al_2O_3	[NH_3]=11400 ppm, [O_2]=8.21%, Flow rate=74.7 mL/min, weight=0.2 g	100%/300 °C	83%/300 °C	2002	4
7.5wt% Ag-2.5wt% Cu/$A_{l2}O_3$	[NH_3]=1000 ppm, [O_2]=10%, Flow rate=50 mL/min, weight=0.1 g	100%/~250 °C	95%/~250 °C	2002	4
10 wt% Ag/Al_2O_3	[NH_3]=1000 ppm, [O_2]=10%, Flow rate=50 mL/min, weight=0.1 g	100%/~200 °C	83%/~200 °C	2003	5
10 wt% Ag/SiO_2	[NH_3]=1000 ppm, [O_2]=10%, Flow rate=50 mL/min, weight=0.1 g	100%/~200 °C	42%/~200 °C	2003	5
10wt% Ag/Al_2O_3	[NH_3]=10000 ppm, [O_2]=10%, Flow rate=400 mL/min, weight=0.8 g	100%/~200 °C	82%/~200 °C	2004	6
5wt% Ag-5wt% Cu/Al_2O_3	[NH_3]=10000 ppm, [O_2]=10%, Flow rate=400 mL/min, weight=0.8 g	100%/~330 °C	95%/~330 °C	2004	6
10wt% Ag/Al_2O_3	[NH_3]=500 ppm, [O_2]=10%, Flow rate=200 mL/min, weight=0.2 g	100%/~150 °C	35%/~150 °C	2009	7
Ag0.1Ce0.1/Al_2O_3	[NH_3]=500 ppm, [O_2]=10%, Flow rate=200 mL/min, weight=0.2 g	100%/160 °C	50%/160 °C	2011	8
Ag-Cu/WMH	[NH_3]=1000 ppm, [O_2]=10%, GHSV=2250 h^{-1}	100%/230 °C	86%/230 °C	2013	9
10wt% Ag/Al_2O_3	[NH_3]=1000 ppm, [O_2]=10%, Flow rate=400 mL/min, weight=0.4 g	100%/200 °C	85%/200 °C	2014	10

Ag/USY	[NH_3]=5000 ppm, [O_2]=2.5%, Flow rate=40 mL/min, SV=15400 h^{-1}	100%/200 °C	94%/200 °C	2016	11
Ag/meso-TiO_2	[NH_3]=5000 ppm, [O_2]=2.5%, Flow rate=40 mL/min, weight=0.1 g	100%/350 °C	86%/350 °C	2017	12
1.5wt%Ag-10wt%Cu/Al_2O_3	[NH_3]=5000 ppm, [O_2]=2.5%, Flow rate=40 mL/min, weight=0.1 g	100%/375 °C	94%/375 °C	2018	13
Ag/SiO_2-TiO_2	[NH_3]=500 ppm, [O_2]=10%, Flow rate=100 mL/min, GHSV=28000 h^{-1}	100%/200 °C	63%/200 °C	2018	14
Ag/nano-Al_2O_3	[NH_3]=500 ppm, [O_2]=10%, Flow rate=100 mL/min, GHSV=28000 h^{-1}	100%/140 °C	71%/140 °C	2018	15
Ag/Al_2O_3-H_2	[NH_3]=500 ppm, [O_2]=10%, Flow rate=100 mL/min, GHSV=28000h^{-1}	100%/180 °C	83%/180 °C	2019	16
Ag/ZSM-5	[NH_3]=1000 ppm, [O_2]=10%, Flow rate=100 mL/min, GHSV=35000 h^{-1}	100%/135 °C	75%/135 °C	2019	17
Ag_2Cu_1 alloy	[NH_3]=1000 ppm, [O_2]=10%, Flow rate=100 mL/min, GHSV=12000 h^{-1}	100%/135 °C	75%/135 °C	2019	17
Ag/MnO_2-300	[NH_3]=50 ppm, [O_2]=20%, Flow rate=100 mL/min, weight=0.15 g	15%/35 °C 100%/75 °C	62%/75 °C	This work	
Ag/MnO_2-400	[NH_3]=50 ppm, [O_2]=20%, Flow rate=100 mL/min, weight=0.15 g	10%/35 °C 100%/90 °C	96%/90 °C 99%/100 °C	This work	

Table S4. Results for calculations of surface number and density of Ag NPs

Catalysts	Weight/g	Surface Ag (wt%) [a]	Ag loadings (wt%) [b]	Surface Ag/μmol	Size of Ag NPs / nm [c]	Number of Ag atoms in Ag NPs [d]	Number of Ag NPs [d]	Density of Ag particles / N nm^{-2}
Ag/MnO_2-80	0.15	7.3	7.3	1015	5.1	2152	2.84E+17	0.047
Ag/MnO_2-200	0.15	6.5	7.3	899	4.0	1395	3.90E+17	0.060
Ag/MnO_2-300	0.15	4.7	7.3	651	3.3	708	4.75E+17	0.086
Ag/MnO_2-400	0.15	4.0	7.3	553	2.4	368	4.48E+17	0.140

[a] Determined by atomic absorption spectra (AAS). 0.5 mol/L HNO_3 was used to dissolve the surface Ag.
[b] They were calcined from the same precursor of Ag/MnO_2-80.
[c] Determined by TEM.
[d] Calculated on the basis of a truncated octahedral model structure reported in reference. [18]

Table S5. Physicochemical properties of Ag/MnO_2-*X* catalysts

Catalysts	Acidity (mmol/g) [a]	H_2 takes (mmol/g) [b]	O_2-TPD (mmol/g)	S_{BET} (m^2/g)
Ag/MnO_2-80	0.31	6.87	1.37	40
Ag/MnO_2-200	0.29	7.60	1.43	43
Ag/MnO_2-300	0.27	7.84	1.47	43
Ag/MnO_2-400	0.30	7.34	1.53	42
Ag/MnO_2-500	0.27	7.17	1.49	40
MnO_2	0.36	7.94	0.89	48

a: Determined by NH_3-TPD

b: Determined by H_2-TPR

2.2. Supplementary catalytic reaction and characterization of Ag/MnO_2 with different Ag loadings

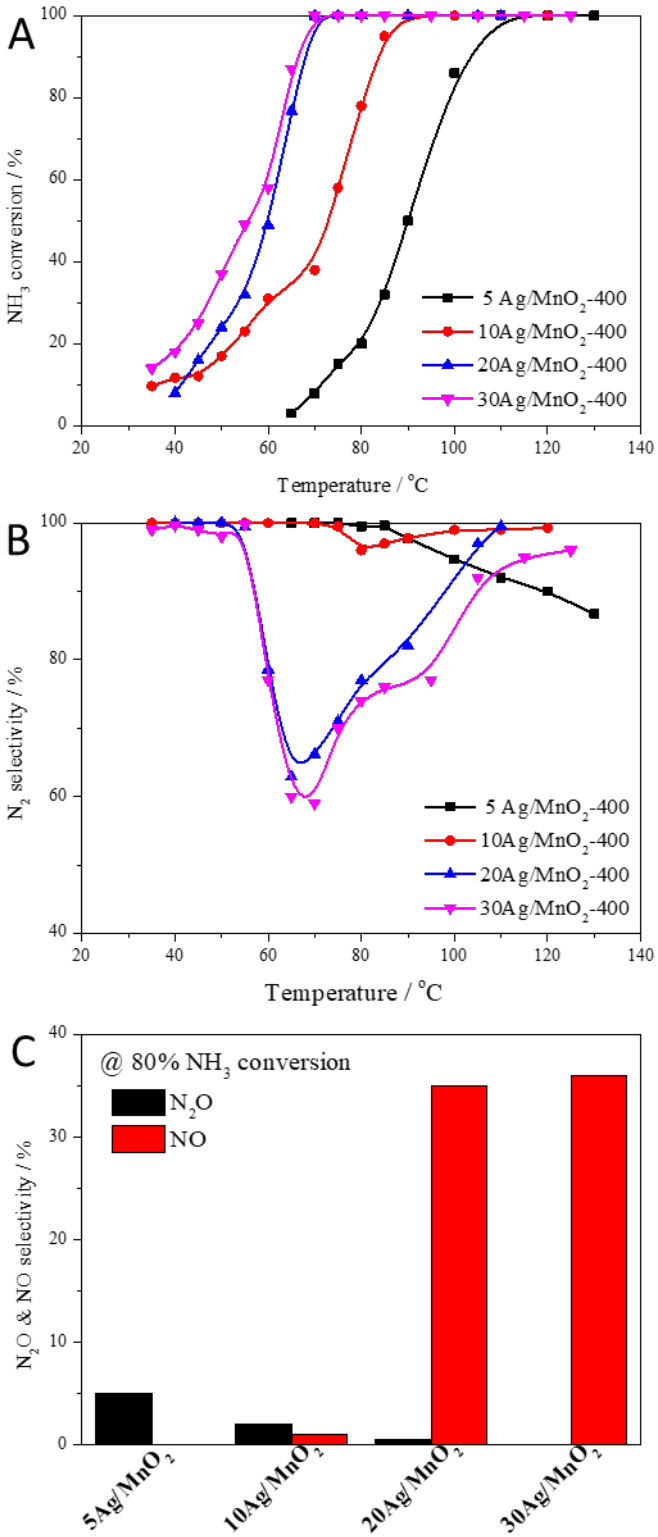

Fig. S14. NH_3-SCO catalytic performance over yAg/MnO_2-400 catalysts: (A) NH_3 conversion results, (B) N_2 selectivity results, and(C) NO and N_2O selectivity results.

NH_3-SCO catalytic reactions over yAg/MnO_2-400 catalyst with different Ag loadings were carried out. As shown in Fig. S14A, it was found that $5Ag/MnO_2$-400 has a low catalytic activity, reaching 100% NH_3 conversion at 110 ^oC. The catalytic activity was increased by increasing Ag loadings from 5% to 30%. $30Ag/MnO_2$-400 showed the highest catalytic activity among the Ag/MnO_2 catalysts with distinct loadings, with almost 20% NH_3 conversion at 40 ^oC and 100% NH_3 conversion at 70 ^oC.

On the other hand, a similar changing tendency of N_2 selectivity as well as NO and N_2O selectivity with Ag/MnO_2-*X* catalysts was found over yAg/MnO_2-400 catalysts. That is, N_2 selectivity first decreased and then increased with increasing temperature. With increase in Ag loading, N_2O selectivity decreased, but NO selectivity increased. As can be seen in Fig. S15, larger Ag NPs were formed with higher Ag loadings. The results strongly suggest that Ag size/structure plays a crucial role in the regulation of N_2 selectivity and type of byproduct.

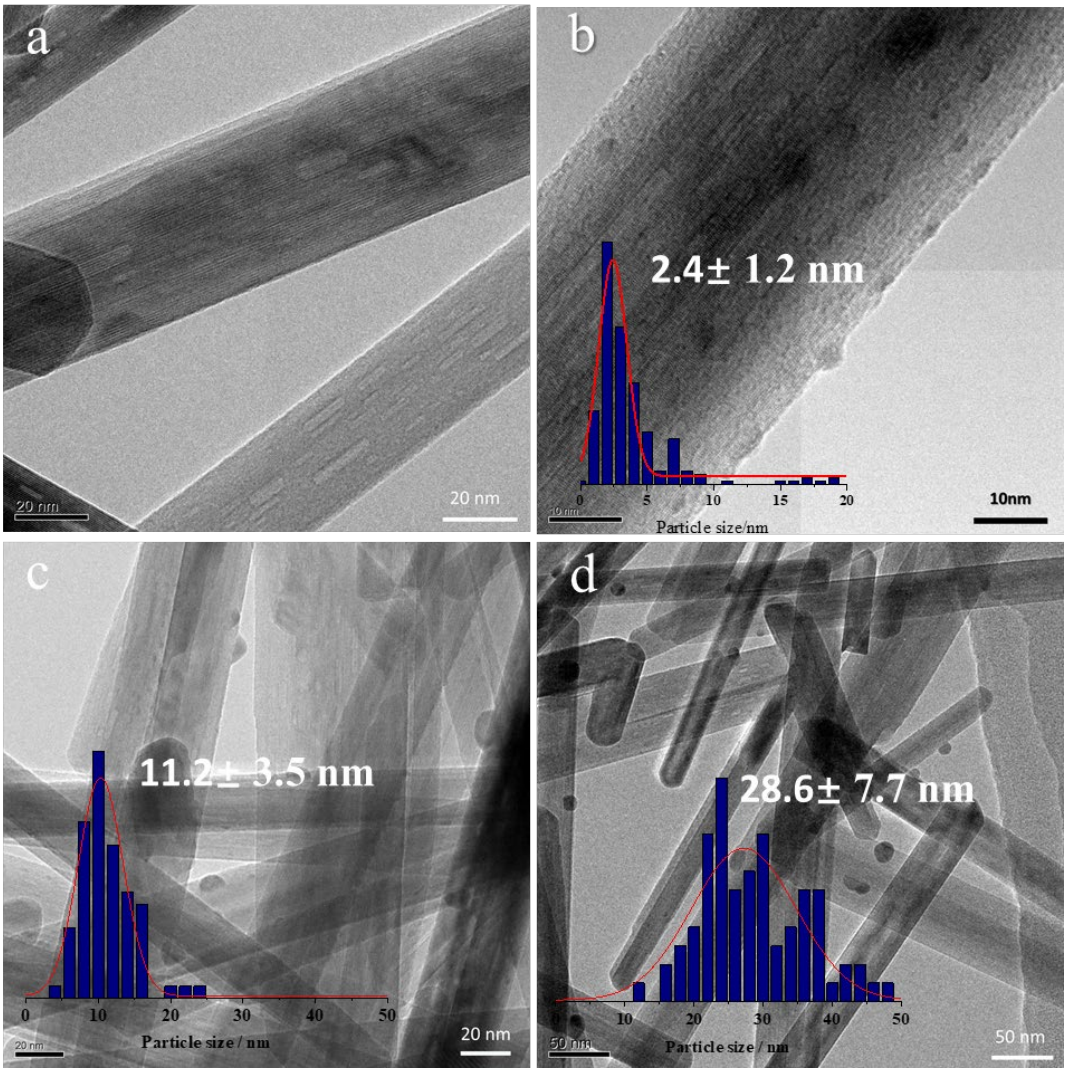

Fig. S15. TEM images of yAg/MnO_2-400 catalysts: (a) 5Ag/MnO_2-400, (b) 10Ag/MnO_2-400, (c) 20Ag/MnO_2-400, and (d) 30Ag/MnO_2-400.

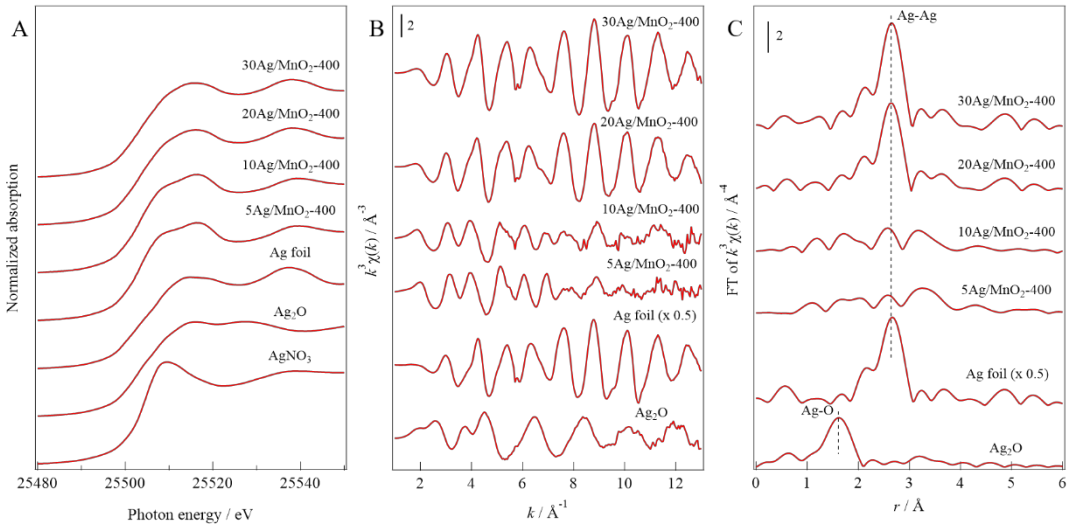

Fig. S16. Ag K-edge XANES spectra (A), k^3-weighted EXAFS oscillation (B), and their Fourier transforms (C) of yAg/MnO_2-400 catalysts and references.

Fig. S16 shows Ag K-edge XANES spectra, k^3-weighted EXAFS oscillation and their Fourier transforms of yAg/MnO_2-400 catalysts and references. The spectral shape of Ag K-edge XANES spectra of yAg/MnO_2-400 catalysts, which was close to that of Ag foil, suggested that Ag species in yAg/MnO_2-400 catalysts were present as metallic state. The white-line intensities of yAg/MnO_2-400 catalysts appeared at 25530 eV, which is slightly higher than that for Ag foil and the height of the white-line gradually decreased with an increase in the Ag loading (Fig. S17). The high intensity of the white-line of yAg/MnO_2-400 suggests the presence of electron-deficient Ag metal NPs.

Fig. S16B and S16C and Table S6 show the EXAFS spectra, their FTs and structural parameters determined by the EXAFS fitting, respectively. In the FTs of the EXAFS spectra of yAg/MnO_2-400 catalysts, the Ag–Ag scattering peak was observed at around 2.7 Å and the height of the Ag-Ag peak shown in Fig. S16C increased with increase in the Ag loading amount. The coordination number of Ag-Ag increased with an increase in the Ag loading amount. Therefore, larger Ag NPs are considered to be formed at larger Ag loading amounts (< 20 wt%).

Table S6. Structural parameters of yAg/MnO_2-400[a]

	CN[b]	r[c] / Å	σ^2[d] / Å^2	ΔE_0[e] / eV	R[f]
5Ag/MnO_2-400	1.800	2.804	0.018	-11.2	0.35
10Ag/MnO_2-400	3.057	2.796	0.018	-10.7	0.35
20Ag/MnO_2-400	5.233	2.849	0.012	-2.9	0.05
30Ag/MnO_2-400	6.318	2.851	0.011	-1.2	0.06
Ag foil	12[g]	2.860	0.011	-0.2	0.11

a Curve fitting analyses of the FTs of EXAFS were performed in R-space between 2.0 and 3.2 Å, and *k*-space between 3.0 and 12.0 Å^{-1}
b Coordination number.
c Distance of Ag–Ag.
d Debye–Waller factor.
e Edge-energy shift.
f *R* factor.
g Fixed.

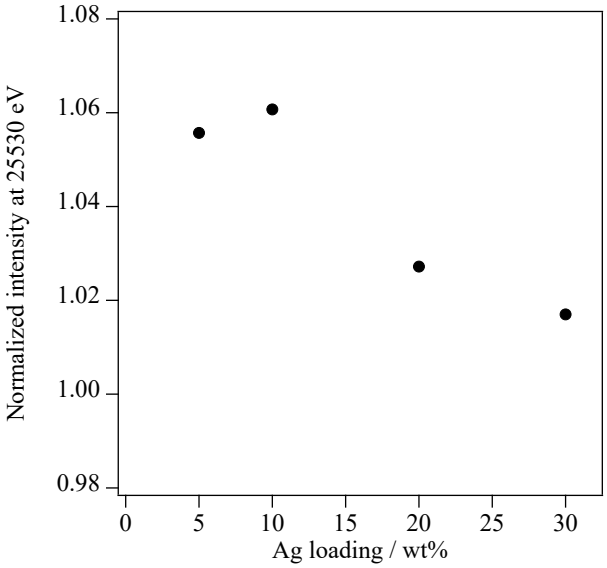

Fig. S17. White-line intensity of Ag K-edge XANES spectra of yAg/MnO_2-400 catalysts at 25530 eV. For Ag foil, the intensity is 0.98566.

3. Supplementary References

1. M.A. Vannice, Kinetics of Catalytic Reactions, in, Springer Science+Business Media, Inc., 2005.
2. B.E. Poling, J. O'Connell, J.M. Prausnitz, The Properties of Gases and Liquids, 5th ed., McGraw-Hill Professional Publishing, New York, NY, USA, 2001.
3. Gang, L.; Anderson, B.; Van Grondelle, J.; Van Santen, R., Intermediate species and reaction pathways for the oxidation of ammonia on powdered catalysts. *J. Catal.*, **2001**, *199* (1), 107-114.
4. Gang, L.; Anderson, B.; Van Grondelle, J.; Van Santen, R.; Van Gennip, W.; Niemantsverdriet, J.; Kooyman, P.; Knoester, A.; Brongersma, H., Alumina-supported Cu–Ag catalysts for ammonia oxidation to nitrogen at low temperature. *J. Catal.*, **2002**, *206* (1), 60-70.
5. Gang, L.; Anderson, B. G.; van Grondelle, J.; van Santen, R. A., Low temperature selective oxidation of ammonia to nitrogen on silver-based catalysts. *Appl. Catal. B-Environ.*, **2003**, *40* (2), 101-110.
6. Yang, M.; Wu, C.; Zhang, C.; He, H., Selective oxidation of ammonia over copper-silver-based catalysts. *Catal. Today*, **2004**, *90* (3-4), 263-267.
7. Zhang, L.; He, H., Mechanism of selective catalytic oxidation of ammonia to nitrogen over Ag/Al_2O_3. *J. Catal.*, **2009**, *268* (1), 18-25.
8. Zhang, L.; Liu. F.; Yu. Y.; Liu. Y.; Zhang, C.; He, H., Effects of adding CeO_2 to Ag/Al_2O_3 catalyst for ammonia oxidation at low temperatures. *Chinese J. Catal.*, **2011**, *32* (5), 727-735.
9. Qu, Z.; Wang, Z.; Quan, X.; Wang, H.; Shu, Y., Selective catalytic oxidation of ammonia to N_2 over wire-mesh honeycomb catalyst in simulated synthetic ammonia stream. *Chem. Eng. J.*, **2013**, *233*, 233-241.
10. Qu, Z.; Wang, H.; Wang, S.; Cheng, H.; Qin, Y.; Wang, Z., Role of the support on the behavior of Ag-based catalysts for NH_3 selective catalytic oxidation (NH_3-SCO). *Appl. Surf. Sci.*, **2014**, *316*, 373-379.
11. Góra-Marek, K.; Tarach, K. A.; Piwowarska, Z.; Łaniecki, M.; Chmielarz, L., Ag-loaded zeolites Y and USY as catalysts for selective ammonia oxidation. *Catal. Sci. Tech.*, **2016**, *6* (6), 1651-1660.
12. Jabłońska, M.; Ciptonugroho, W.; Góra-Marek, K.; Al-Shaal, M. G.; Palkovits, R., Preparation, characterization and catalytic performance of Ag-modified mesoporous TiO_2 in low-temperature selective ammonia oxidation into nitrogen and water vapour. *Microporous Mesoporous Mater.*, **2017**, *245*, 31-44.
13. Jabłońska, M.; Beale, A. M.; Nocuń, M.; Palkovits, R., Ag-Cu based catalysts for the selective ammonia oxidation into nitrogen and water vapour. *Appl. Catal. B*, **2018**, *232*, 275-287.
14. Wang, F.; Ma, J.; He, G.; Chen, M.; Wang, S.; Zhang, C.; He, H., Synergistic Effect of TiO_2-SiO_2 in Ag/Si-Ti catalyst for the selective catalytic oxidation of ammonia. *Ind. Eng. Chem. Res.*, **2018**, *57* (35), 11903-11910.
15. Wang, F.; Ma, J. Z.; He, G. Z.; Chen, M.; Zhang, C. B.; He, H., Nanosize Effect of Al_2O_3 in Ag/Al_2O_3 catalyst for the selective catalytic oxidation of ammonia. *ACS Catal.*, **2018**, *8* (4), 2670-2682.
16. Wang, F.; He, G.; Zhang, B.; Chen, M.; Chen, X.; Zhang, C.; He, H., Insights into the activation effect of H_2 pretreatment on Ag/Al_2O_3 catalyst for the selective oxidation of ammonia. *ACS Catal.*, **2019**, *9* (2), 1437-1445.
17. Wang, Z.; Sun, Q.; Wang, D.; Hong, Z.; Qu, Z.; Li, X., Hollow ZSM-5 zeolite encapsulated Ag nanoparticles for SO_2-resistant selective catalytic oxidation of

ammonia to nitrogen. *Sep. Purif. Technol.*, **2019**, *209*, 1016-1026.
18. Carlsson, A.; Puig-Molina, A.; Janssens, T. V., New method for analysis of nanoparticle geometry in supported fcc metal catalysts with scanning transmission electron microscopy. *J. Phys. Chem. B*, **2006**, *110* (11), 5286-5293.